Cavitating flow about a wedge at incidence

By A. D. COX and W. A. CLAYDEN
Ministry of Supply, Armament Research and Development Establishment, Fort Halstead, Kent

(*Received* 10 *October* 1957)

SUMMARY

A mathematical model is constructed for cavitating flow past a wedge with sides of equal length but with its axis of symmetry placed at an angle to the incident stream. The model involves a subsidiary cavity with a re-entrant jet at the vertex. Only the case of zero cavitation number is considered. The flow field is worked out in some detail for small angles of incidence, and the lift, drag and moment coefficients are calculated as far as first-order terms in the angle of incidence. It is shown that the effect of the rate of loss of momentum in the re-entrant jet on these force coefficients is negligible to this order.

Experimentally, it is shown that the secondary cavity does exist under suitable conditions, and the force coefficients obtained agree with the theory.

1. INTRODUCTION

The problem of two-dimensional steady cavitating flow with zero cavitation number past a symmetrical wedge in an infinite stream, neglecting external forces, has in the past been solved exactly, using complex variable techniques, for the particular case of a non-yawed wedge (see Lamb 1932, or Milne-Thomson 1949).

Milne-Thomson has also derived a solution involving a yawed wedge. He found, however, that for the flow pattern considered it is not possible to specify arbitrarily the ratio of the lengths of the two wedge faces. This ratio is determined as a function of the wedge and yaw angles, and is unity only for zero yaw; so that, in particular, Milne-Thomson's method fails to solve the problem of a symmetric wedge at non-zero yaw.

To be able to specify the ratio of the lengths of the wedge faces independently of the wedge angle and yaw angle, it is necessary to relax the conditions determining Milne-Thomson's problem, and it is clear that the non-essential condition imposed is that which requires the vertex of the wedge to be a stagnation point. This is borne out by considering the special case of a yawed semi-infinite flat plate, whereon the stagnation point is not in general in a symmetric position (see Milne-Thomson 1949).

It is by discarding this condition that the following solution is found, involving a flow pattern which is of a sufficiently novel type to appear to

merit description in some detail. The novel feature of the flow—a subsidiary cavity in the lee of the wedge vertex—is shown experimentally to exist under certain conditions.

2. The physical model of the flow

The method of solution used will be that of the complex variable, and for this we need to assume potential flow and neglect viscosity.

It is convenient to adopt the convention that the angle of incidence is positive, so that the 'lower' face of the wedge is inclined to the stream at a greater angle than the 'upper' face. By analogy with the behaviour in the case of the flat plate, we should expect the stagnation point to move to the lower face of the wedge.

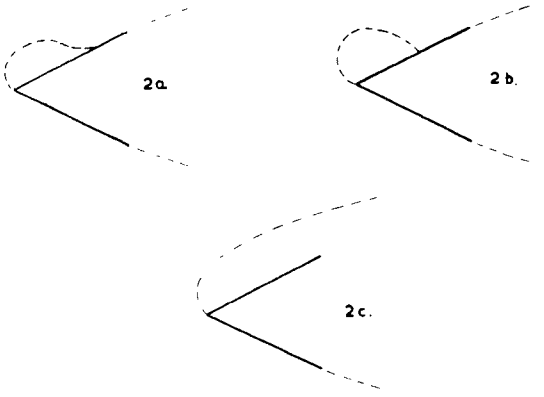

Figure 2.

The dividing streamline through this stagnation point will, on the downstream side, follow the wedge face until it reaches the rear of the wedge and will then become the lower free-streamline of the main or 'rear' cavity. On the upstream side of the stagnation point the dividing streamline will reach the vertex of the wedge and would then, in the absence of a stagnation point, need to attain an infinite fluid velocity to turn round the sharp corner of the wedge. However, owing to the inability of real fluids to sustain pressures less than vapour pressure, a rise in velocity above a certain finite value, in this case taken to be the main stream velocity, is impossible. We shall assume in our model that a cavity will form, bounded by a free-streamline which is the smooth continuation of the dividing streamline. Besides the rear cavity, therefore, we have a 'bubble' cavity formed on the upper face of the wedge; this certainly exists under suitable conditions, as is shown by the photograph (figure 1, plate 1) taken in the A.R.D.E. Cavitation Tunnel.

The free-streamline springing from the vertex must either rejoin the upper face of the wedge or else continue to infinity. The first case might conceivably occur as illustrated in figure 2. If, however, the re-attachment

A. D. Cox and W. A. Clayden, Cavitating flow about a wedge at incidence, Plate I.

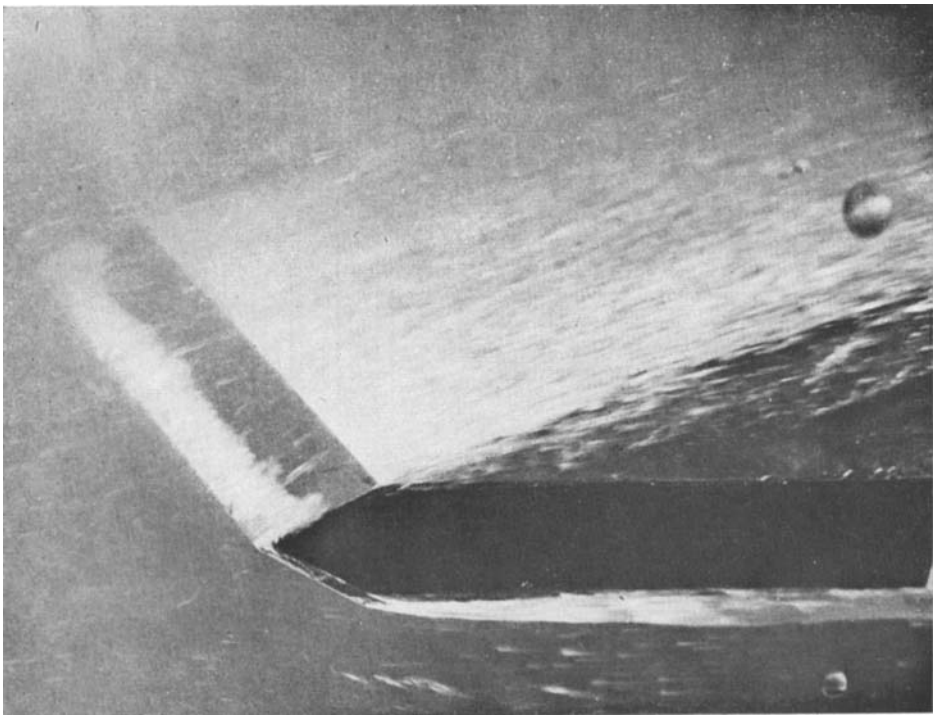

Figure 1. 30° semi-angle wedge.
Angle of incidence = 10°, cavitation number = 0·003.

were effected tangentially, as in figure 2(*a*), the free-streamline would contain a point of inflection, which is impossible because the pressure gradient, and therefore the streamline curvature, must always be directed towards the cavity. If the re-attachment were other than tangential, as in figure 2(*b*), it would involve a stagnation point, which again is impossible on a free-streamline.

If, on the other hand, the free-streamline continues to infinity downstream, so that the upper face of the wedge is included in the cavity, as in figure 2(*c*), then the flow is simply that past a yawed flat plate. This flow pattern will indeed occur under suitable conditions, which may easily be defined from the exact general solution of this type of flow (see Milne-Thomson 1949).

When the dimensions and orientation of the wedge preclude the possibility of 'yawed flat plate' flow, we are left with the possibility that the flow continues to infinity in some other direction. This apparently unreal configuration, involving a double-sheeted flow pattern, is similar to the familiar re-entrant jet models occurring in the solutions obtained by Kreisel (1946) and Shiffman (1949) for non-yawed wedges at non-zero cavitation number.

While Gilbarg & Rock (1946) have shown by numerical methods that drag forces are remarkably insensitive to the assumptions made as to the flow pattern at the rear of the cavity, at least when this region of the flow is far removed from the wetted nose of the body, we cannot quote this as sufficient justification for the model now proposed, since the re-entrant jet is here postulated as forming on the face of the wedge itself. The justification will rest partly on the degree of agreement achieved with experimental results, and partly on the mathematical demonstration that the rate of loss of momentum in the re-entrant jet is of smaller order of magnitude than the drag and lift forces on the wedge, at least for small angles of yaw.

We now consider the assumed mathematical model in detail. Referring to figure 3, we have a symmetrical wedge DCD' of semi-angle β in an infinite stream which makes an angle α with the axis of symmetry of the wedge. As is customary, the uniform stream is considered to be due to a source system at A, the point at infinity (A_1, A_2, etc. all refer to the unique point at infinity in this plane and are labelled differently for the purpose of identification of individual streamlines).

The streamline A_1B divides at the stagnation point B on the lower wedge face CD'. A_1BD' becomes the lower bounding free-streamline $D'A_2$ of the main cavity and A_1BC breaks away smoothly from the vertex C to form the bounding free-streamline CQE of the subsidiary cavity. The free-streamline CQE and part of the flow to its left turn almost completely round and flow to infinity as a separate jet, bounded on one side by the extension of the wedge face DC and on the other side by the free-streamline CQE. The point at infinity on this jet is denoted by E and is quite distinct from A, the point at infinity in the main stream. Since the streamlines

in the jet cut across the streamlines of the main flow pattern, it is necessary to visualize the flow as occurring on a double-sheeted Riemann surface, one sheet of which carries the main flow pattern, while the jet crosses on to the second sheet. The cut dividing one sheet from the other is somewhat arbitrary, but it can be said to have the form $GQPA_3$ shown in figure 3. Since part of the flow to the left of A_1B flows upstream and the rest flows downstream, forming the upper wall of the main cavity, there must be a stagnation point H on the upper face CD of the wedge. The dividing streamline A_5H will, on the downstream side, become the upper bounding free-streamline DA_4 of the main cavity.

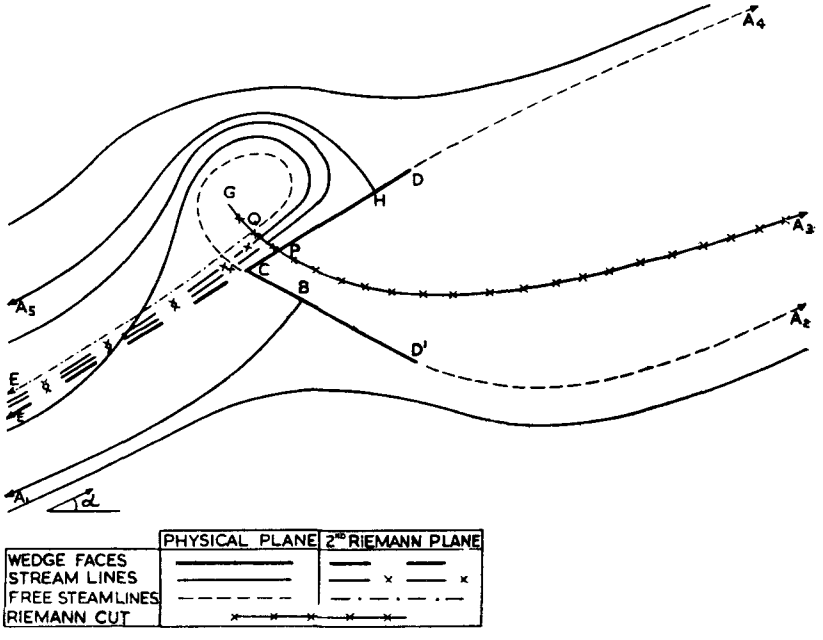

Figure 3. Assumed model of the flow.

Thus, of the fluid flowing from A, that lying to the right of A_1B returns to A, and that to the left of A_1B and to the right of A_5H flows to E and is 'lost', while that to the left of A_5H returns to A.

3. The solution of the problem

We use the standard technique of obtaining conformal transformations between suitable complex variables to determine the flow pattern and all physical quantities.

For the physical plane as represented in figure 3, we use the variable $z = x+iy$, where x and y are rectangular Cartesian coordinates parallel and perpendicular respectively to the plane of symmetry of the wedge, the direction of increasing x being downstream. Next, we define the complex

velocity potential $w = \phi + i\psi$, where ϕ is the velocity potential and ψ the stream function. The velocity vector (u, v) is given by

$$u = \frac{\partial \phi}{\partial x} = \frac{\partial \psi}{\partial y}, \qquad v = \frac{\partial \phi}{\partial y} = -\frac{\partial \psi}{\partial x}.$$

By a suitable choice of scale in the w-plane, in respect to the as yet undetermined length scale, we arrange that

$$u_\infty^2 + v_\infty^2 = 1,$$

where (u_∞, v_∞) is the velocity vector of the flow at infinity. Then

$$dw/dz = u - iv = qe^{-i\theta},$$

where $$q^2 = u^2 + v^2 \quad \text{and} \quad \theta = \tan^{-1} v/u.$$

The w-plane is illustrated in figure 4. All the streamlines, since they are by definition lines of constant ψ, become lines parallel to the ϕ-axis. The pair of streamlines HDA, HE and the pair BCE, $BD'A$ should each actually be represented by a single straight line but are shown separated for convenience.

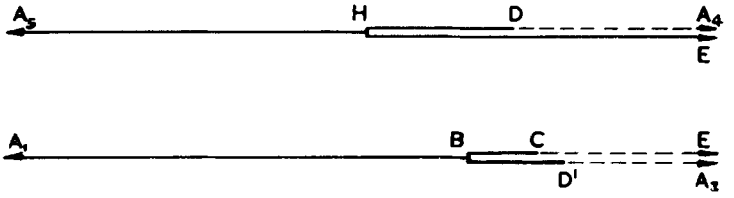

Figure 4. The complex velocity potential.

The next variable is the logarithmic hodograph variable Ω defined by

$$\Omega = \log(dw/dz) = \log q - i\theta.$$

This variable is plotted in figures 5 (*a*) and (*b*). The free-streamlines $D'AD$ and CQE are lines of constant speed q, this constant speed being equal to that at infinity so that, by our choice of scale, we have $q = 1$ (i.e. $\log q = 0$) on the free-streamlines. Thus in the Ω-plane they become portions of the imaginary axis. Since the wedge faces CB, BD' and DH, HE are lines of constant θ, they become lines parallel to the real Ω-axis with a discontinuity of amount π in the imaginary part of Ω at H and B, where $Re(\Omega) = -\infty$.

It is found on tracing the other streamlines that the Ω-plane is doubly-covered. To overcome this we make a cut in the Ω-plane from the point R, where $d\Omega/dz$ vanishes, to the point at infinity in the Ω-plane in a negative direction, and then consider the Ω-plane as a Riemann surface with two sheets cross-joined along this line.

Then the streamlines are as shown in figures 5 (*a*) and (*b*), where, for convenience, we have separated the two Riemann sheets. The streamlines themselves show how the four half-planes are joined. The images of all streamlines between the dividing streamlines A_1B and A_5H of figure 3 lie between AX_1 and AX_2 in figure 5 (*a*); after crossing the cut they remain on the second sheet, eventually terminating at E in figure 5 (*b*).

In order to obtain the requisite conformal transformations between these variables, we define an auxiliary variable τ by requiring that the streamlines DAD', $D'BC$, CQE, EHD become the sides of the rectangle

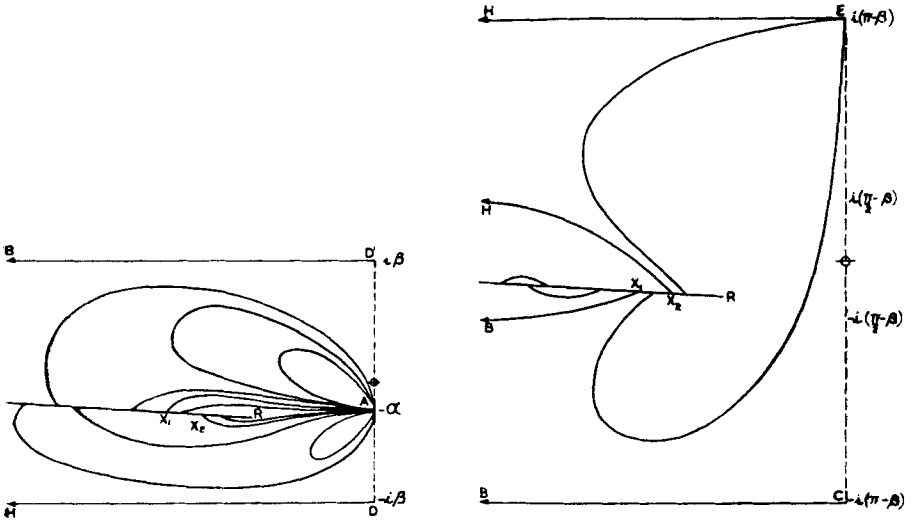

Figure 5. The logarithmic hodograph.

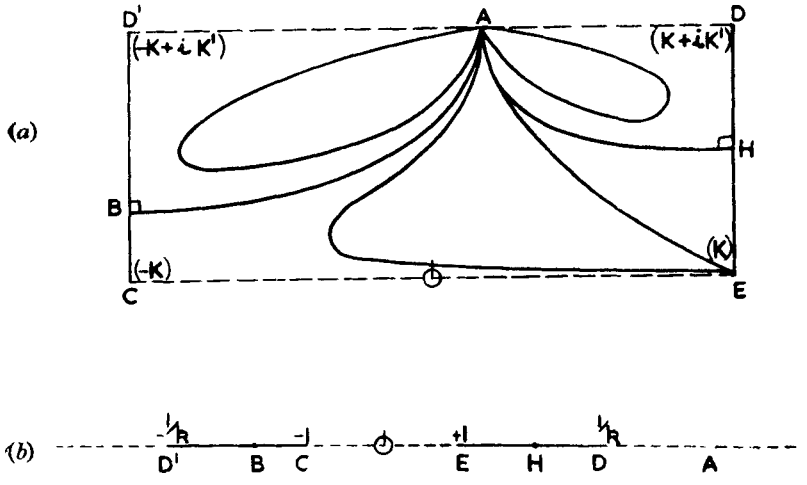

Figure 6. (*a*) τ-plane, (*b*) t-plane.

formed by the four points $\tau = \pm K, \pm K+iK'$, the orientation of the lines being as shown in figure 6(*a*). We also suppose the points H, B, A to be represented by

$$\left.\begin{aligned} \tau_H &= +K+ih, \\ \tau_B &= -K+ib, \end{aligned}\right\} \qquad K' \geqslant h, b \geqslant 0$$

$$\tau_A = iK'+a, \qquad -K \leqslant a \leqslant K.$$

In this plane the streamlines are as shown in figure 6(*a*), the behaviour near A being precisely as in figure 5(*a*) apart from a change of orientation.

We now find by inspection the conformal transformations which transform the lines DAD', $D'BC$, CE, EHD and AB, AH into their images in the w- and Ω-planes. From this we shall find a parametric relation between w and dw/dz, and hence the problem is solved.

The Ω–τ transformation

The functions to be used in this and the following transformation, as has been foreshadowed by choice of the τ-plane, are the Jacobian elliptic functions, for the definitions and properties of which reference may be made to Neville (1951), Jahnke & Emde (1948), Milne-Thomson (1950), and Whittaker & Watson (1940). Although Neville's notation is certainly the more elegant, we have used that of Whittaker & Watson as being the more familiar.

The function $d\Omega/d\tau$ must have a simple pole at τ_H and τ_B and must also be purely imaginary all along the boundary rectangle in the τ-plane. It must also be finite and non-zero at τ_A. The transformation

$$\frac{d\Omega}{d\tau} = \frac{T_1 \operatorname{sn}\tau}{\operatorname{sn}\tau - \operatorname{sn}\tau_H} + \frac{T_2 \operatorname{sn}\tau}{\operatorname{sn}\tau - \operatorname{sn}\tau_B} + iN, \tag{1}$$

where N is real and T_1, T_2 are purely imaginary, satisfies all these requirements since $\operatorname{sn}\tau$ is real all along the rectangle in the τ-plane. The function $d\Omega/d\tau$ can be shown to have only one zero inside the rectangle and this must obviously be at τ_R, where R is the branch point illustrated in figure 5.

To ensure that the transformation gives the correct scales as well as directions we have to impose further conditions. The first two are that Ω must have a discontinuity of $i\pi$ at τ_H and τ_B, and these are easily seen to lead to

$$T_1 = \operatorname{cn}\tau_H \operatorname{ds}\tau_H, \qquad \text{and} \qquad T_2 = \operatorname{cn}\tau_B \operatorname{ds}\tau_B.$$

The other conditions are

$$\Omega_D = -i\beta, \quad \Omega_{D'} = i\beta, \quad \Omega_C = -i(\pi-\beta), \quad \Omega_E = i(\pi-\beta), \quad \Omega_A = -i\alpha,$$

and these must be applied to the integrated form of equation (1). Integrating, we get

$$\Omega = \Pi(\tau, \tau_H - iK') + \Pi(\tau, \tau_B - iK') - \\ - \tfrac{1}{2}\log\left\{\frac{\operatorname{cd}\tau_H + \operatorname{cd}\tau}{\operatorname{cd}\tau_H - \operatorname{cd}\tau}\,\frac{\operatorname{cd}\tau_B + \operatorname{cd}\tau}{\operatorname{cd}\tau_B - \operatorname{cd}\tau}\right\} + iN\tau, \tag{2}$$

where

$$\Pi(x,y) = \int_0^x \frac{k^2 \operatorname{sn}y \operatorname{cn}y \operatorname{dn}y \operatorname{sn}^2 u}{1 - k^2 \operatorname{sn}^2 y \operatorname{sn}^2 u}\, du,$$

as defined by Whittaker & Watson (1940). The constant of integration in (2) is zero due to the skew symmetry of the conditions at C and E.

The first four conditions imply that

$$NK = (\pi-\beta) + i[\Pi(K, \tau_H - iK') + \Pi(K, \tau_B - iK')],$$

and

$$\beta K' = \tfrac{1}{2}\pi(h+b). \tag{3}$$

The fifth condition gives

$$-i\alpha = \Pi(a, \tau_H - iK') + \Pi(a, \tau_B - iK') + ia\{Z'(h) + Z'(b)\} - \\ -i\left\{\tan^{-1}\frac{k\,\mathrm{sc}'b}{\mathrm{dc}\,a} - \tan^{-1}\frac{k\,\mathrm{sc}'h}{\mathrm{dc}\,a}\right\} + \\ + i\tan^{-1}\left\{-\frac{(k')^2\,\mathrm{sn}\,a\,\mathrm{sn}'h\,\mathrm{cn}'h}{\mathrm{cn}\,a\,\mathrm{dn}\,a\,\mathrm{dn}'h}\right\} + \\ + i\tan^{-1}\left\{-\frac{(k')^2\,\mathrm{sn}\,a\,\mathrm{sn}'b\,\mathrm{cn}'b}{\mathrm{cn}\,a\,\mathrm{dn}\,a\,\mathrm{dn}'b}\right\}, \quad (4)$$

where the prime indicates that the co-modulus k' replaces the modulus k, and $Z(x)$ is the Jacobian zeta function.

The w–τ transformation

This transformation is more easily found by considering a further auxiliary variable t defined by $t = \mathrm{sn}\,\tau$. Since $\mathrm{sn}\,\tau$ is real all along the rectangle in the τ-plane, the t-plane is as in figure 6(*b*).

Then, using the Schwartz–Christoffel theorem, we see that we require the following conditions for dw/dt:

(i) It should have a simple zero at t_H, t_B.

(ii) It should have a simple pole at t_E and a triple pole at t_A.

Thus we get

$$\frac{dw}{dt} = \frac{P(t-t_H)(t-t_B)}{(t-t_E)(t-t_A)^3},$$

or, in terms of τ,

$$\frac{dw}{d\tau} = \frac{P\,\mathrm{cn}\,\tau\,\mathrm{dn}\,\tau(\mathrm{sn}\,\tau - \mathrm{sn}\,\tau_H)(\mathrm{sn}\,\tau - \mathrm{sn}\,\tau_B)}{(\mathrm{sn}\,\tau - 1)(\mathrm{sn}\,\tau - \mathrm{sn}\,\tau_A)^3} \quad (5)$$

since $$\mathrm{sn}\,\tau_E = \mathrm{sn}\,K = 1.$$

The constant P determines the length scale in the problem, and it is in relation to this that we choose the scale in the w-plane so that $q_\infty = 1$.

Equation (5) may be integrated to give w as a function of τ. Also, since $\Omega = \log(dw/dz)$, equations (2) and (5) together yield an expression for $dz/d\tau$ which can again be integrated to give z as a function of τ. Thus we can determine w and z parametrically in terms of τ, and hence find the flow pattern. From these we can determine all the physical quantities required.

4. Determination of parameters

There are four parameters a, b, h and k in the problem. Equations (3) and (4) show that specifying the wedge semi-angle and the angle of yaw will provide two equations. The other two conditions to be imposed are the following:

(i) The lengths of the sides of the wedge must be in a predetermined ratio. In particular we shall consider a symmetrical wedge.

(ii) In general C will not lie on the continuation of DH. Ensuring that it does provides the fourth condition and makes the solution determinate.

Conditions (i) and (ii) can be expressed in the mathematical form

$$DD' = 0 + 2i|CD'|\sin\beta, \tag{6}$$

where DD' and CD' are conveniently calculated by integrating $dz/d\tau$ along the sides of the rectangle in the τ-plane. The real and imaginary parts of this equation, together with equations (3) and (4), provide the four equations necessary for determining the four parameters of the problem.

In general these quantities will have to be determined numerically, but in certain cases, and in particular when k is small, the calculations can be carried out analytically as far as first-order terms. Since it can be shown that small k combined with certain other assumptions corresponds to small angles of yaw, a situation of particular interest, we shall consider this case in more detail.

5. The limiting case of small angles of yaw: the flow pattern in the large

As the yaw tends to zero, it is reasonable to suppose that the flow pattern studied here will tend to the familiar symmetrical flow pattern. In other words, the effect of the existence of the secondary cavity on the main cavity should tend to zero as the yaw tends to zero. Similarly the secondary cavity must become so small that its detailed geometry is unaffected by the main cavity. Thus the two free-streamlines must tend to become independent of one another, or, interpreting this in the τ-plane, $K'/K \to \infty$ as the yaw tends to zero. From the theory of Jacobian elliptic functions, this implies that k tends to zero.

Now, writing $2\beta/\pi = \epsilon$, where $0 < \epsilon < 1$, equation (3) becomes

$$h + b = \epsilon K',$$

and, since $h, b \geqslant 0$,

$$h \leqslant \epsilon K', \qquad b \leqslant \epsilon K'. \tag{7}$$

Writing $\sigma = iK' - \tau$, we transform the two fundamental equations (1) and (5) into the form

$$\frac{d\Omega}{d\sigma} = -\frac{\operatorname{cn}\sigma_H \operatorname{ds}\sigma_H}{1 - \operatorname{ns}\sigma_H \operatorname{sn}\sigma} - \frac{\operatorname{cn}\sigma_B \operatorname{ds}\sigma_B}{1 - \operatorname{ns}\sigma_B \operatorname{sn}\sigma} - iN, \tag{8}$$

and

$$\frac{dw}{d\sigma} = \frac{Pk \operatorname{sn}^3\sigma_A \operatorname{cn}\sigma \operatorname{dn}\sigma (1 - \operatorname{ns}\sigma_H \operatorname{sn}\sigma)(1 - \operatorname{ns}\sigma_B \operatorname{sn}\sigma)}{(1 + k \operatorname{sn}\sigma)(\operatorname{sn}\sigma_A - \operatorname{sn}\sigma)^3}. \tag{9}$$

When $k \to 0$, and provided σ lies on or near DAD', the following relations hold:

$$\operatorname{sn}\sigma = \sin\sigma[1 + O(k^2)], \qquad \operatorname{cn}\sigma = \cos\sigma[1 + O(k^2)], \qquad \operatorname{dn}\sigma = 1 + O(k^2).$$

Moreover, it is easily shown from (7) that

$$\operatorname{ns}\sigma_B = O(k^n), \qquad \operatorname{ns}\sigma_H = O(k^n),$$
$$\operatorname{cn}\sigma_B \operatorname{ds}\sigma_B = -i + O(k^{2\epsilon}), \qquad \operatorname{cn}\sigma_H \operatorname{ds}\sigma_H = -i + O(k^{2\epsilon}),$$

where $$1 > n = 1-\epsilon > 0.$$

Equations (8) and (9) therefore reduce to the form

$$d\Omega/d\sigma = M - i\mu \sin\sigma + O(k^\gamma), \tag{10}$$

and $$\frac{dw}{d\sigma} = \frac{S\cos\sigma}{(\sin\sigma+\sin a)^3}[1+\mu\sin\sigma+O(k^\gamma)], \tag{11}$$

where $$\mu = -\operatorname{ns}\sigma_H - \operatorname{ns}\sigma_B = O(k^n),$$

and M, S, γ are constants, γ being chosen as the smaller of the two quantities 1 or $2n$.

Integrating (10), and applying the conditions at D and D', we obtain

$$e^{-\Omega} = e^{-i\epsilon\sigma}[1 - i\mu\cos\sigma + O(k^\gamma)]. \tag{12}$$

Since $\exp(-\Omega) = dz/dw$, we find that

$$\frac{dz}{d\sigma} = S\frac{\cos\sigma}{(\sin\sigma+\sin a)^3}e^{-i\epsilon\sigma}[1 - i\mu e^{i\sigma} + O(k^\gamma)].$$

Hence

$$DD'[1+O(k^\gamma)] = S\oint_{-\pi/2}^{\pi/2}\frac{\cos\sigma}{(\sin\sigma+\sin a)^3}[e^{-i\epsilon\sigma} - i\mu e^{i\eta\sigma}]\,d\sigma, \tag{13}$$

the path of integration being the straight line from $-\pi/2$ to $\pi/2$, indented on the positive side by a small semi-circle described about $\sigma = -a$.

From the condition (6), expressing the equality of the wedge faces, it follows that $Re(DD') = 0$. Applying this condition to (13), we find that

$$a = \mu/t(\epsilon) = O(k^n),$$

the derivation of this formula, and the definition of $t(\epsilon)$, being given in Appendix I. The function $t(\epsilon)$ varies monotonically from $4/(4-\pi) = 4{\cdot}660$ at $\epsilon = 0$ to $5{\cdot}000$ at $\epsilon = 1$ (as shown in table 1, § 6).

When this condition is satisfied we have

$$|DD'| = S\sin(\tfrac{1}{2}\epsilon\pi)F(\epsilon)[1+O(k^\gamma)],$$

where $F(\epsilon) = 1+\epsilon+\frac{1}{2}\epsilon^2[\psi(1-\epsilon/4)-\psi(1/2-\epsilon/4)]$, $\psi(x)$ being the digamma function ($\psi(x) = (d/dx)\Gamma(x)$). In particular, $F(0) = 1$ and $F(1) = 2+\pi/2$.

In order to determine the forces on the wedge, let us consider a circle in the σ-plane, given by $\sigma = -a + re^{i\eta}$ (r small). In the z-plane this corresponds to a large contour completely surrounding the wedge and enclosing most of the flow, as shown in figure 7.

Then, equating the forces acting on this contour to the rate of change of momentum inside it, we have

$$(X, Y) = \rho\int(\mathbf{n}\,.\,\mathbf{q})\mathbf{q}\,\mathrm{d}s - \int p\mathbf{n}\,\mathrm{d}s + \mathbf{R},$$

where (X, Y) is the force per unit length acting on the wedge, $\mathbf{n}$ is the unit vector along the outward normal to the contour, s measures arc length

along the contour, ρ is the density, p is the pressure, $\mathbf{q}$ is the velocity vector (u, v), and $\mathbf{R}$ is the contribution of the fluid in the re-entrant jet.

Referring to figure 7, we know that on QSP, $\mathbf{q} = 0$, $p = p_\infty$; and on PRQ, $\mathbf{q}$ is known, $p = p_\infty + \frac{1}{2}\rho(1-q^2)$. Hence

$$(X, Y) = \rho \int_\Lambda (\mathbf{n}.\mathbf{q})\mathbf{q}\, ds - \tfrac{1}{2}\rho \int_\Lambda (1-q^2)\mathbf{n}\, ds + \mathbf{R},$$

where Λ is the semicircle $\sigma = -a + re^{i\eta}$, $0 \leqslant \eta \leqslant \pi$.

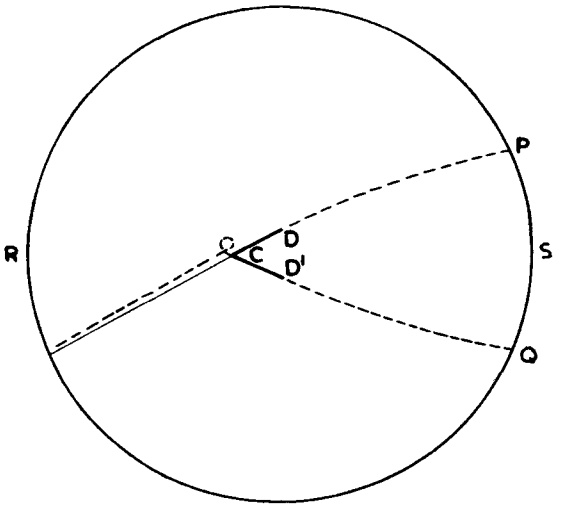

Figure 7.

Since the left-hand side of this equation is independent of r, so also is the right-hand side. Thus, on letting r tend to zero, we find

$$X = \tfrac{1}{2}\epsilon^2\pi S\rho + R_1 + O(a^2),$$

and

$$Y = \tfrac{1}{2}a\pi\rho S[-t + \epsilon(2t-1) - \epsilon^2 t + \epsilon^3] + R_2 + O(a^2),$$

where R_1 and R_2 are the components of $\mathbf{R}$.

From (12) we find, on putting $\sigma = -a$, that the angle of incidence α is given by

$$\alpha = a\{\epsilon - t\} + O(a^2).$$

Hence the drag force D and the lift force L per unit length are given by

$$D = X + O(\alpha^2) = \tfrac{1}{2}\epsilon^2\pi\rho S + R_1 + O(\alpha^2),$$

and

$$L = Y - X\alpha + O(\alpha^2) = \tfrac{1}{2}a\pi\rho S[-t + \epsilon(2t-1)] + R_2 - \alpha R_1 + O(\alpha^2).$$

In a similar manner we can find the pitching moment M per unit length, measured about the mid-point of the base of the wedge, and reckoned as positive for a destabilizing moment. Using the formula

$$M = \int p(x\, dx + y\, dy) - \rho \int (vx - uy)(u\, dx - v\, dy),$$

we find that

$$M = -\tfrac{1}{2}\rho\pi a S^2 p(\epsilon) + R_3 + O(\alpha^2) \qquad (14)$$

where R_3 represents the term due to the re-entrant jet, and the function $p(\epsilon)$ is explained in Appendix III. In particular we have

$$p(0) = 3/(8-2\pi), \qquad \text{and } p(1) = -3/2.$$

The terms R_1, R_2 and R_3, representing the effect of the re-entrant jet, must be small if our mathematical model is to be physically realistic. In the next section we shall prove that they do, in fact, become negligible compared with the other terms in D, L and M as α tends to zero.

6. The flow pattern in the neighbourhood of the vertex and its effect on the forces acting on the wedge

The analysis of the preceding section was effected without making any assumptions regarding the behaviour of b and h as k tends to zero, apart from the restriction given in equation (7). It is now necessary to examine their behaviour in more detail, and it is clear that three possibilities arise:

(i) b and h both tend to infinity;

(ii) b remains finite; or

(iii) h remains finite.

The correct choice is governed by the fact that we have yet to satisfy the condition imposed by the imaginary part of equation (6), representing the fact that C must be collinear with D and H. (The real part of this equation has already been satisfied by the condition $\mu = a\,t(\epsilon)$ in the previous section.)

Since the analysis differs in detail for the three different possibilities, we shall reproduce here only that corresponding to case (iii) above, since, as we shall show, this is the case that enables equation (6) to be satisfied.

In this case it follows from (3) that $b/K' \to \epsilon$, and hence

$$\mathrm{ns}\,\tau_B \sim \mathrm{nc}\,\tau_B = O(k^{\epsilon}), \qquad \text{and } \mathrm{dn}\,\tau_B = 1 + O(k^{2n}).$$

Then on or near CE it can be shown, from (1), that

$$\frac{d\Omega}{d\tau} = \frac{\cos\tau_H}{\sin\tau - \sin\tau_H} + iZ + O(k^{\epsilon}),$$

where Z is a real constant.

Integrating, and applying the conditions at C and E, we find

$$e^{-\Omega} = -i\frac{\cos\frac{1}{2}(\tau+\tau_H)}{\sin\frac{1}{2}(\tau-\tau_H)}\,e^{-in\tau}[1+O(k^{\epsilon})].$$

Similarly, from (5),

$$\frac{dw}{d\tau} = +\frac{4^{\epsilon}Sk^{1+n}\cos\tau(\sin\tau-\sin\tau_H)}{2(\sin\tau-1)}\,[1+O(k^{\epsilon})].$$

Hence

$$\frac{dz}{d\tau} = +i4^{\epsilon}\frac{Sk^{1+n}}{2}\,e^{-in\tau}\,\frac{1+\sin\tau}{\cos\tau}\,[1+\cos(\tau+\tau_H)][1+O(k^{\epsilon})]. \tag{15}$$

Now the imaginary part of equation (6), implying the collinearity of C, D and H, may be replaced by the following condition:

$$Im\left\{\overrightarrow{CE}e^{-i\beta}\right\} = g, \tag{16}$$

where E is the point at infinity on the free-streamline of the re-entrant jet, and g is the width of the re-entrant jet at infinity.

But g may be readily evaluated by studying the behaviour of equation (15) in the neighbourhood of $\tau = K = \pi/2 + O(k^2)$; thus

$$g = \tfrac{1}{2}Sk^{1+n}\pi[1+\sin\tau_H][1+O(k^\epsilon)]. \tag{17}$$

Substituting in (15), our condition becomes

$$\pi[\cosh h - 1][1+O(k^\epsilon)] = \int_0^\pi (1+\cos t)(\sin t)^{-1}(\sin nt - \\ - \cosh h \cos t \sin nt - \sinh h \sin t \cos nt)\, dt, \tag{18}$$

where we have written $\tau = \pi/2 - t$.

In Appendix II this equation is solved explicitly and then, using equation (15), the dimensions of the subsidiary bubble are calculated. However, as we shall now show, the effect of the value of h on the forces is negligible.

Equation (17) gives the value of g and it is obvious without actual evaluation that the values of R_1 and R_2 will both be equal to multiples of g, the multipliers being of order unity as α tends to zero. However, g itself is of order $\alpha^{1+1/n}$, so that we have

$$D = \tfrac{1}{2}\epsilon^2\pi\rho S + O(\alpha^2), \tag{19}$$

$$L = \tfrac{1}{2}a\pi\rho S[-t+\epsilon(2t-1)] + O(\alpha^2), \tag{20}$$

$$M = -\tfrac{1}{2}a\rho\pi S^2 p(\epsilon) + O(\alpha^2). \tag{21}$$

We now define a drag coefficient and lift and pitching moment slope coefficients, using the dynamic head as the reference pressure and the combined length of the wedge faces $c = |DD'|\operatorname{cosec}\beta$ as the reference length. An asterisk will be used to distinguish these coefficients from those which would be obtained by taking $|DD'|$ itself as the reference length. The advantage in taking c as reference length is that all these coefficients tend to finite limits as ϵ tends to zero.

Using an obvious notation, we obtain

$$C_D^* = \frac{D}{\tfrac{1}{2}\rho q_\infty^2 c} = \frac{\epsilon^2\pi}{F(\epsilon)} + O(\alpha^2), \tag{19'}$$

$$\left[\frac{\partial C_L^*}{\partial\alpha}\right]_{\alpha=0} = \lim_{\alpha\to 0}\left[\frac{L}{\tfrac{1}{2}\rho q_\infty^2 \alpha c}\right] = \frac{\pi[-t+\epsilon(2t-1)]}{(\epsilon-t)F(\epsilon)}, \tag{20'}$$

$$\left[\frac{\partial C_M^*}{\partial\alpha}\right]_{\alpha=0} = \lim_{\alpha\to 0}\left[\frac{M}{\tfrac{1}{2}\rho q_\infty^2 \alpha c^2}\right] = \frac{-\pi p(\epsilon)}{(\epsilon-t)F^2(\epsilon)}. \tag{21'}$$

It is interesting to compare these formulae with known limiting values as α tends to zero and as β tends to zero or $\pi/2$, bearing in mind, however, that the foregoing analysis is not strictly valid when β equals zero or $\pi/2$

For the case α equals zero (19′) agrees with the formula given by Perry (1952), while (20) and (21) give zero values for L and M as would be expected.

When ϵ tends to unity, corresponding to a flat plate nearly perpendicular to the stream, (20′) agrees with the value given by Milne-Thomson (1949), and (21′) with that given by Lamb (1932).

When ϵ tends to zero, corresponding to a flat plate nearly parallel to the stream, we find that (20′) gives a value π and (21′) a value $3\pi/8$. These do not agree with the classical values for cavitating flat plates, but this is to be expected since even in the limiting case both sides of the wedge are wetted. A more reasonable comparison is with a flat plate at incidence in fully wetted flow, with circulation chosen using the Joukowsky hypothesis of a finite velocity at the trailing edge. In this case Ramsey (1947) gives the value π for $[\partial C_L^*/\partial\alpha]_{\alpha=0}$ and $3\pi/8$ for $[\partial C_M^*/\partial\alpha]_{\alpha=0}$, so that again agreement is secured with classical theory.

Table 1 gives values of C_D^*, $[\partial C_L^*/\partial\alpha]_{\alpha=0}$ and $[\partial C_M^*/\partial\alpha]_{\alpha=0}$ and they are plotted in figures 8 and 9 respectively.

ϵ	$t(\epsilon)$	C_D^*	$\left[\frac{\partial C_L^*}{\partial\alpha}\right]_{\alpha=0}$	$\left[\frac{\partial C_M^*}{\partial\alpha}\right]_{\alpha=0}$
0	4·660	0	3·142	1·178
0·2	4·721	0·102	1·711	0·553
0·4	4·785	0·325	0·629	0·117
0·6	4·853	0·571	−0·138	−0·053
0·8	4·924	0·770	−0·628	−0·110
1·0	5·000	0·880	−0·880	−0·092

Table 1.

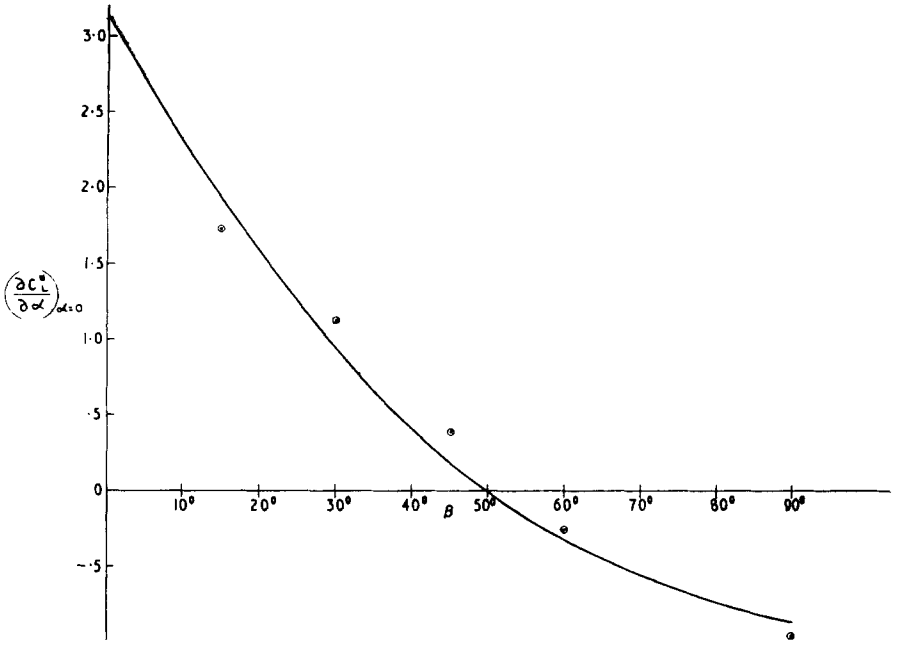

Figure 8. Modified lift slope coefficient as a function of β.

7. Experimental method

As a result of the foregoing theoretical study of cavitating flow about a wedge at incidence, experimental data were needed to verify the assumption

made concerning the existence of the subsidiary cavity formed on the upper face of the wedge, and also to measure the hydrodynamic forces acting on the wedge. These data were obtained in the A.R.D.E. cavitation tunnel (see Clayden 1954).

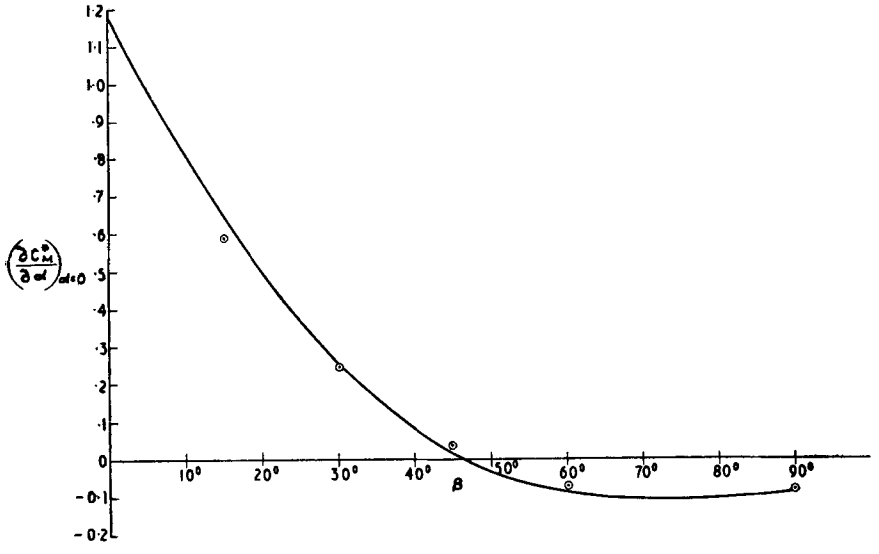

Figure 9. Modified moment slope coefficient as a function of β.

This tunnel is a re-circulating type with a rectangular 9×7 in. free jet working section with fixed vertical side walls and free top and bottom surfaces. The working section speed is nominally constant at 40 ft./sec, and the cavitation number is varied by varying the pressure. Very low cavitation numbers ($\sim 0{\cdot}01$) may be obtained in this manner. The basic instrumentation consists of the following:

(1) a horizontal beam manometer to measure the pressure across the contraction nozzle, which is used as a Venturi meter;

(2) a tilting dead weight manometer to measure the difference between the ambient and cavity pressure;

(3) a tilting dead weight manometer to measure the ambient pressure in the working section. This instrument is also used to operate a servo-mechanism to control the tunnel pressure in the range 1 atmosphere to 10 mm of mercury;

(4) a thermocouple thermometer; and

(5) a mechanical three-moment balance.

(The first four instruments give continuous recordings.)

The 30° semi-angle wedge shown in figure 1 (plate 1) was originally used to obtain design data for struts and model supports. It completely spanned the tunnel, but was attached only to the rear boundary wall of the working section. It was used to obtain photographs of the flow pattern, in preference to the family of wedges used to obtain force data, because it permitted an uninterrupted view.

The size of the models used to obtain the force data were as follows: for the wedge semi-angle $\beta = 15°$, the width of the base of the wedge was 0·5 in.; for $\beta = 30°$, 45°, 60° and 90°, the width of the base was 0·3 in. To obtain the force measurements, the wedges were pivoted on the front boundary of the free jet and were attached to the three-moment balance by a universal joint (figure 10). The three-moment balance was mounted on the back of the working section. (A more detailed description of the experimental rig was given by Clayden (1957).) A pressure tap was fitted in the boundary wall of the working section to measure the cavity pressure directly, since the cavity pressure is normally higher than the vapour pressure, due to a small quantity of air leaking through from the balance.

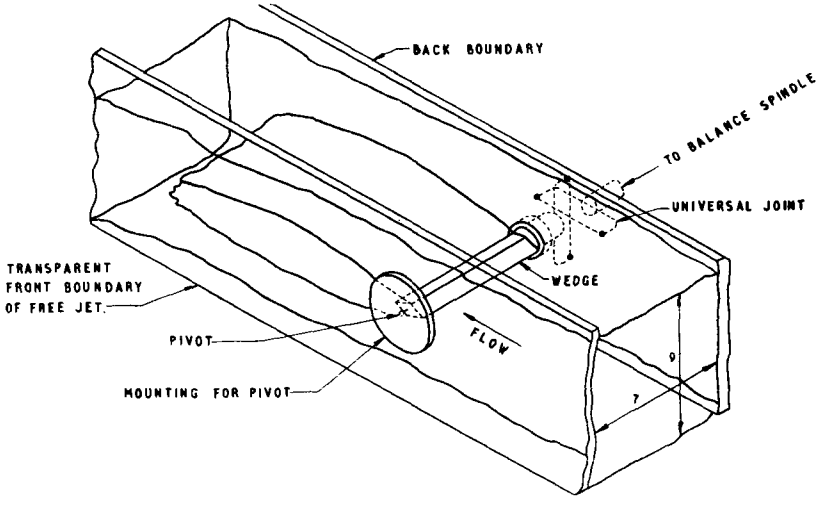

Figure 10. Test rig. Dimensions in inches.

For a typical series of tests the cavitation number was held constant whilst the balance was rotated from $-15°$ to $+15°$ with the horizontal, readings of the three moments being taken at intervals of 3°. Since the angle the free jet makes with the model is not precisely known, the position of zero incidence was determined as the position at which the measured lift force changed sign.

Although the tunnel is capable of achieving a cavitation number as low as 0·01, the lower limit in these tests was determined by the length of the cavity, which for the lowest cavitation numbers extended throughout the length of the working section.

8. Results

Observations and photographs of the flow about a yawed wedge indicated that the mathematical model, illustrated in figure 3, closely resembled a time average of the actual physical flow (figure 1, plate 1). The subsidiary cavity, however, oscillated considerably with a high frequency (a similar cyclic process has been observed and studied by Knapp (1956) for flow along a cylinder with a cavitating head). As the angle of yaw of the wedge

is increased so the subsidiary cavity becomes larger until it finally breaks away leaving the leeward face completely unwetted. The angle at which this occurs has been studied by Clayden (1957) for a family of wedges of varying vertex angles. The force measurements given in this paper are for small angles of incidence with the leeward face at least partially wetted (figure 3).

β	σ	C_{D0}	d	$\frac{\partial C_L}{\partial \alpha}$	$\frac{\partial C_M}{\partial \alpha}$
15°	0·067	0·291	0·00742	0·128	0·157
	0·096	0·300		0·126	0·163
	0·119	0·296		0·124	0·159
	0·170	0·345		0·130	0·163
	0·230	0·361		0·141	0·172
30°	0·059	0·517		0·0423	0·0182
	0·073	0·523	−0·000305	0·0389	0·0172
	0·112	0·536		0·0436	0·0192
	0·134	0·548		0·0435	0·0198
	0·183	0·590		0·0438	0·0198
	0·206	0·608		0·0431	0·0188
45°	0·081	0·681	−0·000342	0·0105	0·00180
	0·116	0·709		0·0097	0·00150
	0·149	0·727		0·0098	0·00212
	0·180	0·755		0·0088	0·00180
	0·260	0·794		0·0097	0·00242
60°	0·116	0·843	−0·00032	−0·00501	−0·00185
	0·122	0·864		−0·00523	−0·00214
	0·164	0·890		−0·00517	−0·00248
	0·210	0·885		−0·00578	−0·00302
	0·268	0·942		−0·00488	−0·00240
90°	0·104	0·945	−0·000170	−0·0171	−0·00214
	0·130	0·974		−0·0174	−0·00166
	0·145	0·991		−0·0170	−0·00148
	0·180	1·025		−0·0171	−0·00165
	0·220	1·056		−0·0168	−0·00231

Table 2.

The force measurements obtained from the three-moment balance were analysed to give C_D, C_L and C_M, the drag, lift and moment coefficients respectively. These results were fitted by the method of least squares to give the following relations for each combination of vertex angle and cavitation number:

$$C_L = (\partial C_L/\partial\alpha)\alpha, \qquad C_M = (\partial C_M/\partial\alpha)\alpha,$$
$$C_D = C_{D0}(1 + d\alpha^2) \qquad (d \text{ constant for a given vertex angle}),$$

where

$C_L = L/\frac{1}{2}\rho q_\infty^2 W$, $C_D = D/\frac{1}{2}\rho q_\infty^2 W$, $C_M = M/\frac{1}{2}\rho q_\infty^2 W^2$, $C_{D0} = C_D$ for $\alpha = 0$.

The results obtained for $\partial C_L/\partial\alpha$, $\partial C_M/\partial\alpha$, C_{D0} and d are tabulated in table 2.

These results are plotted in figures 11, 12 and 13. The values of C_{D0} are compared with theoretical values given by Perry (1952) in figure 11. In order to compare the experimental values of the lift slope coefficient $\partial C_L/\partial\alpha$,

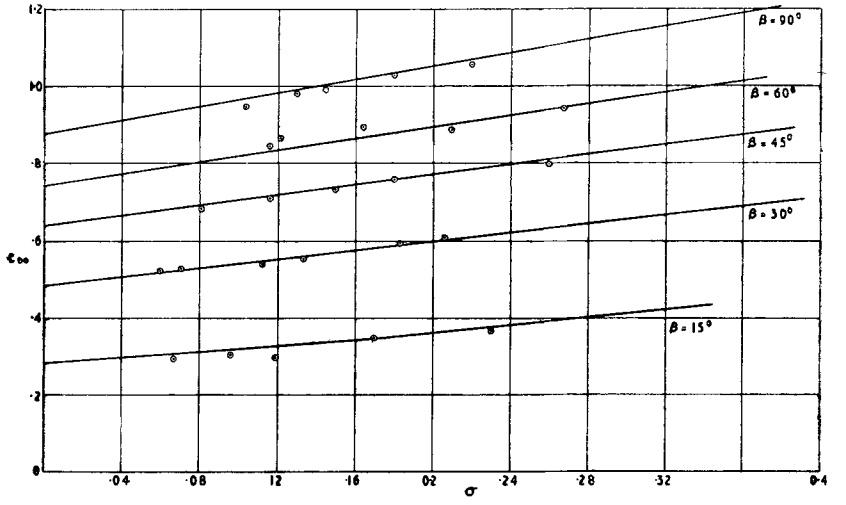

Figure 11. Measured drag coefficient as a function of σ.

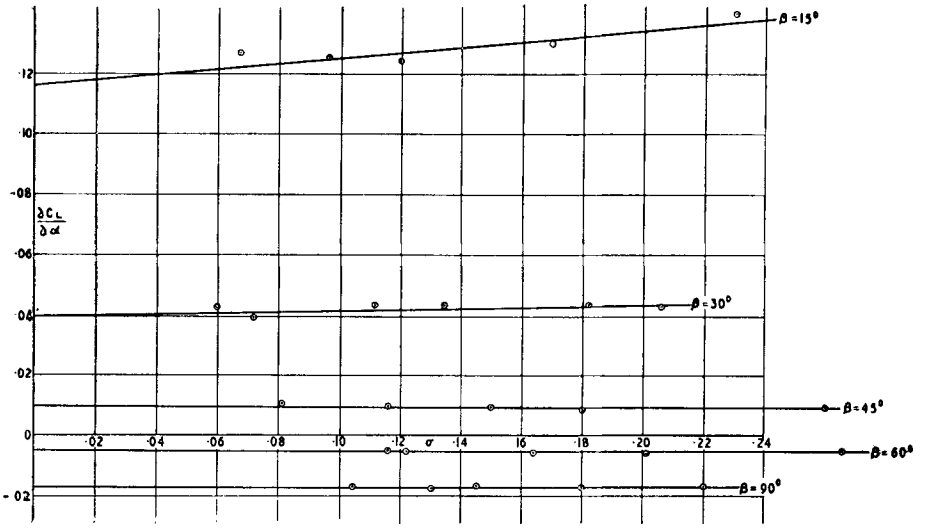

Figure 12. Measured lift slope coefficient as a function of σ.

with the theory developed in this paper, the results are extrapolated to give $(\partial C_L/\partial\alpha)$ for $\sigma = 0$. For values of $\beta = 90°$, $60°$ and $45°$, there does not appear to be any dependence on cavitation number and accordingly the

results are averaged. For $\beta = 30°$ and 15°, however, there is a significant increase of $\partial C_L/\partial\alpha$ with the cavitation number σ, and a least squares fit is used to obtain $(\partial C_L/\partial\alpha)_{\sigma=0}$. The results for the moment coefficient are all fitted with a least squares fit to give $(\partial C_M/\partial\alpha)_{\sigma=0}$. The values of $(\partial C_L^*/\partial\alpha)_{\sigma=0}$ and $(\partial C_M^*/\partial\alpha)_{\sigma=0}$ are compared with theory in figures 8 and 9. These results are tabulated in table 3.

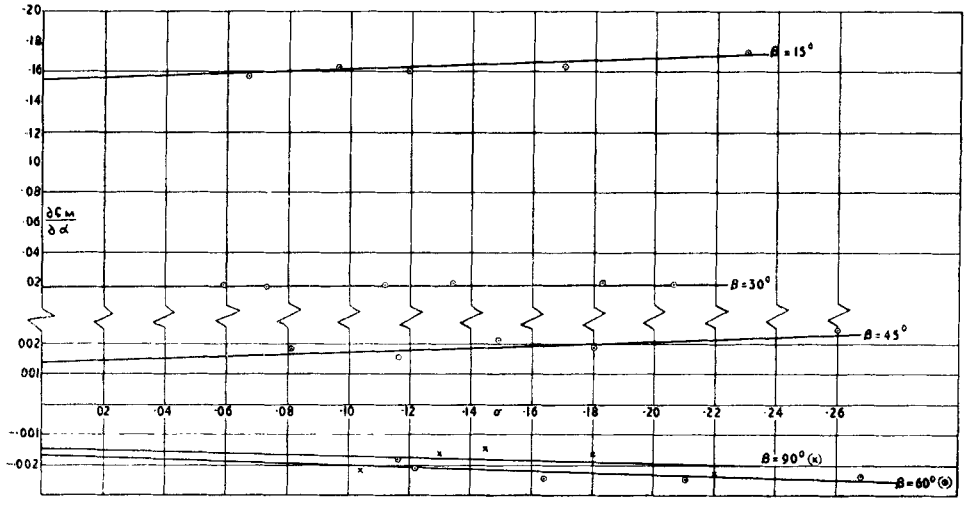

Figure 13. Measured moment slope coefficient as a function of σ.

β	$\dfrac{\partial C_L}{\partial\alpha}$	$\dfrac{\partial C_M}{\partial\alpha}$	$\left[\dfrac{\partial C_L^*}{\partial\alpha}\right]_{\sigma=0}$	$\left[\dfrac{\partial C_M^*}{\partial\alpha}\right]_{\sigma=0}$
15°	$0{\cdot}116+0{\cdot}093\sigma$	$0{\cdot}154+0{\cdot}085\sigma$	1·72	0·582
30°	$0{\cdot}0398+0{\cdot}0192\sigma$	$0{\cdot}0174+0{\cdot}0112\sigma$	1·14	0·248
45°	0·0097	$0{\cdot}00133+0{\cdot}0038\sigma$	0·392	0·038
60°	−0·0052	$-(0{\cdot}00165+0{\cdot}0030\sigma)$	−0·258	−0·071
90°	−0·0171	$-(0{\cdot}00148+0{\cdot}0023\sigma)$	−0·98	−0·085

Table 3.

9. Discussion of results

The drag results for zero incidence plotted in figure 11 show good agreement with theory. No theory is presently available for the dependence of the drag on the angle of incidence except for the case of a flat plate at zero cavitation number, when for a flat plate almost normal to the stream

the drag coefficient may be expressed as $C_D = C_{D0}(1 - 0{\cdot}000238\alpha^2)$ compared with an experimental value of $C_D = C_{D0}(1 - 0{\cdot}000171\alpha^2)$ for α in the range 0–15°.

Since the lift coefficient of a flat plate nearly normal to the stream may be expressed as $C_D \tan\alpha$ (neglecting skin friction), and as C_D behaves as $1+\sigma$, it would seem reasonable to suppose that the lift coefficient would behave in a similar manner. However, the experimental results do not show this trend, and the reason for this discrepancy is not yet apparent. The extrapolated values of the lift slope coefficient have been plotted in figure 8 for comparison with theory when it will be seen that agreement is fair, part of the difference between theory and experiment being accounted for by the fact that insufficient results were obtained to achieve great accuracy in the extrapolated values.

The values of the moment slope coefficient plotted in figure 9 show good agreement with theory. In particular, the negative moment for β greater than 45° is confirmed.

10. Conclusions

The analysis, for small angles of yaw, of the model described in § 2, has been shown to lead to a drag coefficient which differs only by second-order terms in the yaw from that given by the classical solution for a non-yawed wedge, and to lift and moment coefficients which have not previously been calculated, except for a flat plate, where agreement is again secured.

The experiments demonstrated the existence of a subsidiary cavity at the vertex which appeared to be of a cyclic nature, alternately filling with water, breaking away from the vertex, and reforming again. However, the steady state model described will give a first approximation to the time average of the forces, the quantities that were measured in the experiments.

The experiments could not be undertaken at zero cavitation number, but the extrapolated value of the lift slope and moment slope coefficients show reasonable agreement with theory developed in this paper. Good agreement between theory and experiment for the drag coefficient at zero incidence is also secured and experiments confirm the theoretical prediction that the drag for small angles of incidence differs only by small second-order terms in the angle of incidence from the drag at zero incidence.

Since the predictions of this theory are so well in accord with experiment, the theory has since been extended to cover the case of non-zero cavitation number (Cox 1957).

The authors wish to express their thanks to Mr A. H. Armstrong for his guidance and assistance and to Miss K. M. Stocks and her staff for carrying out the numerical work.

Appendix I

The evaluation of the integral I occurring in equation (13)

Expanding in powers of a by Taylor's theorem, and assuming that μ is of the same order of magnitude as a, we find that

$$I = i\sin(\tfrac{1}{2}\epsilon\pi)[1+\epsilon+\tfrac{1}{2}\epsilon^2\{\psi(1-\tfrac{1}{4}\epsilon)-\psi(\tfrac{1}{2}-\tfrac{1}{4}\epsilon)\}]+ \\ +[-3aL_1+\mu L_2+3aL_3+\mu L_4]+O(a^2),$$

where
$$\psi(x) = (d/dx)\log\Gamma(x),$$
$$L_1 = \oint_{-\pi/2}^{\pi/2}\cos\sigma\cos\epsilon\sigma\sin^{-4}\sigma\,d\sigma,$$
$$L_2 = \oint_{-\pi/2}^{\pi/2}\cos\sigma\sin(1-\epsilon)\sigma\sin^{-3}\sigma\,d\sigma,$$
$$L_3 = \epsilon(1-\epsilon^2)\pi/6,$$
$$L_4 = (1-\epsilon)^2\pi/2.$$

By integrating L_2 twice by parts, we find that

$$L_2 = -\cos(\tfrac{1}{2}\epsilon\pi)-\tfrac{1}{4}(1-\epsilon)^2[I_{2-\epsilon}-I_\epsilon],$$

where
$$I_n = \int_{-\pi/2}^{\pi/2}\sin n\theta(\sin\theta)^{-1}\,d\theta,$$
$$= -\cos(\tfrac{1}{2}n\pi)[G(n)-G(-n)],$$

with
$$G(n) = \tfrac{1}{2}[\psi(\tfrac{1}{4}-\tfrac{1}{4}n)-\psi(\tfrac{3}{4}-\tfrac{1}{4}n)].$$

Thus we see that

$$L_2 = -\tfrac{1}{2}(1-\epsilon)^2\pi-\cos(\tfrac{1}{2}\epsilon\pi)[2-\epsilon+(1-\epsilon)^2G(\epsilon)].$$

Similarly, integrating L_1 twice by parts, we find that

$$L_1 = -\tfrac{2}{3}\cos(\tfrac{1}{2}\epsilon\pi)+\tfrac{1}{3}\epsilon L_2-\tfrac{1}{6}\epsilon(1-\epsilon)[I_\epsilon-I_{2-\epsilon}],$$

so that

$$L_1 = \epsilon(1-\epsilon^2)\pi/6-\tfrac{1}{3}\cos(\tfrac{1}{2}\epsilon\pi)[2-\epsilon^2-\epsilon(1-\epsilon^2)G(\epsilon)].$$

Thus, on applying condition (6), we find that

$$\mu = at(\epsilon),$$

where
$$t(\epsilon) = \frac{2-\epsilon^2-\epsilon(1-\epsilon^2)G(\epsilon)}{2-\epsilon+(1-\epsilon)^2G(\epsilon)}.$$

This result is consistent with our original assumption that μ and a are of the same order of magnitude.

Appendix II

(*a*) *The calculation of* $h = h(n)$

We have, from equation (18),

$$\pi[\cosh h-1] = J_1(n)-\cosh hJ_2(n)-\sinh hJ_3(n). \qquad \text{(II.1)}$$

where

$$J_1(n) = \int_0^\pi\frac{1+\cos t}{\sin t}\sin nt\,dt, \qquad J_2(n) = \int_0^\pi\frac{1+\cos t}{\sin t}\sin nt\cos t\,dt,$$

and
$$J_3(n) = \int_0^\pi\frac{1+\cos t}{\sin t}\cos nt\sin t\,dt.$$

The substitution $t = 2\mu$ leads immediately to

$$J_1(n) = \tfrac{1}{2}[I_{2n+1} + I_{2n-1}],$$

in the notation of Appendix I, and hence

$$J_2(n) + J_3(n) = J_1(n+1) = \tfrac{1}{2}[I_{2n+3} + I_{2n+1}],$$
$$J_2(n) - J_3(n) = J_1(n-1) = \tfrac{1}{2}[I_{2n-1} + I_{2n-3}].$$

Solving equation (II.1) for e^h, we find the values given in table 4.

(*b*) *The dimensions of the subsidiary cavity*

We have, from equation (15), on writing $2^{2\epsilon-2}Sk^{1+n}Z = ze^{-i\beta}$ and $\tau = \pi/2 - t$,

$$\frac{dZ}{dt} = -\frac{1+\cos t}{\sin t} e^{int} [1 - \cos(t - ih)].$$

If we write $Z = X + iY$, then X is the variable along the top face of the wedge and Y the variable perpendicular to it.

Then the maximum value Y_m of Y is the dimension of the subsidiary cavity perpendicular to the top face of the wedge, and is given by

$$Y_m = -\int_{\pi}^{t_m} \frac{1+\cos t}{\sin t} [\sin nt\,(1 - \cos t \cosh h) - \cos nt \sin t \sinh h]\, dt,$$

where t_m is the value of t where the expression in square brackets vanishes.

The variable X has, for $n > \frac{1}{2}$, two turning points X_1 and X_2 and the dimension of the cavity along the top wedge face is $|X_1 - X_2|$; while, for $n < \frac{1}{2}$, there is one turning point X_3, the dimension of the cavity then being X_3. It is seen that X_1, X_2, and X_3 are given by

$$X_1, X_2, X_3 = -\int_{\pi}^{t_1, t_2, t_3} \frac{1+\cos t}{\sin t} [\cos nt\,(1 - \cos t \cosh h) + \sin nt \sin t \sinh h]\, dt,$$

the appropriate value of t being taken as the upper limit.

Numerically we find the values in table 4.

n	e^h	Y_m	$\lvert X_1 - X_2 \rvert$	X_3
0	1·00000	0	—	2·000
0·2	1·19825	0·343	—	1·925
0·4	1·38439	0·693	—	1·767
0·6	1·54252	1·004	1·526	—
0·8	1·65503	1·221	1·296	—
1·0	1·70711	1·298	1·106	—

Table 4.

Appendix III

The function $p(\epsilon)$ occurring in equation (14) is defined by

$$p(\epsilon) = p_1(\epsilon) + t(\epsilon) p_2(\epsilon),$$

where

$$p_1(\epsilon) = -5\epsilon/24 - \epsilon^3/4 - \epsilon^5/6 + 3\epsilon^2 d_3(\epsilon) + \epsilon(1 - \epsilon^2) a_3(\epsilon)$$
$$p_2(\epsilon) = 1/24 + \epsilon/6 - 3\epsilon^2/4 + \epsilon^3/2 - \epsilon^2 a_3(1 - \epsilon) + (1 - \epsilon)^2 a_3(\epsilon),$$

wherein

$$a_3(\lambda) = \tfrac{1}{3} + \int_{-\pi/2}^{0} \frac{\cos\sigma[\cos\lambda\sigma - 1 + \frac{1}{2}\lambda^2\sin^2\sigma]}{\sin^3\sigma}\, d\sigma$$

and

$$d_3(\lambda) = \lambda/3 + \int_{-\pi/2}^{0} \frac{\cos\sigma[\sin\lambda\sigma - \lambda\sin\sigma - \frac{1}{3}\lambda\{1-\lambda^2\}\sin^3\sigma]}{\sin^4\sigma}\, d\sigma.$$

Computed values of $a_3(\epsilon)$, $a_3(1-\epsilon)$ and $d_3(\epsilon)$ are given in table 5.

ϵ	$a_3(\epsilon)$	$a_3(1-\epsilon)$	$d_3(\epsilon)$
0·0	0·3333	0·4299	0·0000
0·2	0·3386	0·4034	0·0544
0·4	0·3537	0·3764	0·1122
0·6	0·3764	0·3537	0·1766
0·8	0·4034	0·3386	0·2498
1·0	0·4299	0·3333	0·3333

Table 5.

References

Clayden, W. A. 1954 *Unpublished Ministry of Supply Report.*

Clayden, W. A. 1957 *Unpublished Ministry of Supply Report.*

Cox, A. D. 1957 *Unpublished Ministry of Supply Report.*

Gilbarg, D. & Rock, D. H. 1946 On two theories of plane potential flow with finite cavities, *U.S. Naval Ordnance Lab. Mem.* no. 8718.

Jahnke, E. & Emde, F. 1948 *Tables of Functions*, 4th (rev.) Ed. Leipzig: Teubner.

Knapp, R. T. 1956 Further studies of the mechanics and damage potential of fixed type cavities, *Proc. Symposium on Cavitation in Hydrodynamics.* London: H.M.S.O.

Kreisel, G. 1946 Cavitation with finite cavitation number, *Admiralty Research Lab. Rep. U.B.R.C.* 52.

Lamb, H. 1932 *Hydrodynamics*, 6th Ed. Cambridge University Press.

Milne-Thomson, L. M. 1949 *Theoretical Hydrodynamics*, 2nd Ed. London: Macmillan.

Milne-Thomson, L. M. 1950 *Jacobian Elliptic Function Tables.* New York: Dover.

Neville, E. H. 1951 *Jacobian Elliptic Functions*, 2nd Ed. Oxford University Press.

Perry, B. 1952 Evaluation of the integrals occurring in the cavity theory of Plesset and Shaffer, *Cal. Inst. Tech. Hydrodynamics Lab. Rep.* no. 21–11.

Ramsey, A. S. 1947 *A Treatise on Hydromechanics*, Part II. London: Bell.

Shiffman, M. 1949 On free boundaries of an ideal fluid, Part II, *Comm. Pure Appl. Math.* **2**, 1.

Whittaker, E. T. & Watson, G. N. 1940 *A Course of Modern Analysis*, 4th Ed. Cambridge University Press.